Structure and thermal properties of yttrium alumino-phosphate glasses

2008 J. Phys.: Condens. Matter 20 115204

(http://iopscience.iop.org/0953-8984/20/11/115204)

J. Phys.: Condens. Matter **20** (2008) 115204 (13pp) doi:10.1088/0953-8984/20/11/115204

Structure and thermal properties of yttrium alumino-phosphate glasses

Richard A Martin[1], **Philip S Salmon**[1,4], **Donna L Carroll**[2], **Mark E Smith**[2] **and Alex C Hannon**[3]

[1] Department of Physics, University of Bath, Bath BA2 7AY, UK
[2] Department of Physics, University of Warwick, Coventry CV4 7AL, UK
[3] ISIS Facility, Rutherford Appleton Laboratory, Chilton, Didcot, Oxon OX11 0QX, UK

Received 14 December 2007
Published 20 February 2008
Online at stacks.iop.org/JPhysCM/20/115204

Abstract

The structure and thermal properties of yttrium alumino-phosphate glasses, of nominal composition $(Y_2O_3)_{0.31-z}(Al_2O_3)_z(P_2O_5)_{0.69}$ with $0 \lesssim z \lesssim 0.31$, were studied by using a combination of neutron diffraction, ^{27}Al and ^{31}P magic angle spinning nuclear magnetic resonance, differential scanning calorimetry and thermal gravimetric analysis methods. The Vickers hardness of the glasses was also measured. The data are compared to those obtained for pseudo-binary Al_2O_3–P_2O_5 glasses and the structure of all these materials is rationalized in terms of a generic model for vitreous phosphate materials in which Y^{3+} and Al^{3+} act as modifying cations that bind only to the terminal (non-bridging) oxygen atoms of PO_4 tetrahedra. The results are used to help elucidate the phenomenon of rare-earth clustering in phosphate glasses which can be reduced by substituting Al^{3+} ions for rare-earth R^{3+} ions at fixed modifier content.

(Some figures in this article are in colour only in the electronic version)

1. Introduction

Rare-earth phosphate glasses display a host of interesting properties and have a variety of optoelectronic and laser applications [1–6]. It is therefore important to know the structure of these materials in order to understand the interactions between the rare-earth ions and their mediation by the matrix material. This presents, however, a challenging experimental task owing to the inherent structural disorder of a glass and, even in the simplest material, there are at least three different chemical species (rare-earth R, phosphorus P and oxygen O) which leads to a description of the structure in terms of six overlapping pair-correlation functions. A variety of different structural probes has therefore been applied and there has been a recent focus on measuring the R–R pair-distribution function by using methods such as isomorphic substitution in neutron diffraction [7, 8], magnetic difference neutron diffraction [9], anomalous dispersion neutron diffraction [10, 11], and anomalous x-ray scattering [12]. Moreover, glasses with enhanced chemical durability and mechanical properties are routinely prepared by the incorporation of alumina (Al_2O_3) [6, 13] and there is evidence to suggest that the proximity of the rare-earth ions, and hence their degree of clustering, can be controlled by changing the ratio of rare-earth oxide R_2O_3 to Al_2O_3 at fixed P_2O_5 content [7, 8, 14]. The presence of aluminium as a fourth chemical species does, however, further complicate the problem by a need to describe the glass structure in terms of an additional four pair-correlation functions.

It is therefore advantageous to tackle the structure of a given set of these materials by using several different experimental techniques in order to maximize the information that can be obtained. We have chosen to investigate glasses of nominal composition $(Y_2O_3)_{0.31-z}(Al_2O_3)_z(P_2O_5)_{0.69}$, with $0 \lesssim z \lesssim 0.31$, by using a combination of neutron diffraction, ^{27}Al magic angle spinning (MAS) nuclear magnetic resonance (NMR) and ^{31}P MAS NMR spectroscopy. Although Y^{3+} is not from the rare-earth series, it has the same charge as Dy^{3+} and Ho^{3+}, the same ionic radius as Ho^{3+} at 0.90 Å [15], and very similar structural chemistry to Dy^{3+} and Ho^{3+} as indicated by the Pettifor chemical parameter which is comparable for these ions [16]. Y^{3+} is therefore representative of ions from the *small* radius end of the rare-earth series but is non-paramagnetic which makes feasible a detailed study of Y_2O_3–Al_2O_3–P_2O_5 glasses by using ^{27}Al and ^{31}P MAS NMR

[4] Author to whom any correspondence should be addressed.

Table 1. The number y of added modifier oxygen atoms per P_2O_5 unit, the coordination number of the modifying cation $\bar{n}^{O}_{M}$, the number of terminal oxygen atoms O_T available per modifying cation $^{avail}\bar{n}^{O}_{M}$, the parameter f_M, and the shortest M–M nearest-neighbour distance r_{MM} (min) for several crystalline phosphates containing trivalent modifying cations. The ionic radius of M^{3+} in a six-fold coordination environment is 0.535, 0.900, 0.890 and 1.032 Å for Al^{3+}, Y^{3+}, Er^{3+} and La^{3+}, respectively [15].

Crystal	y	$\bar{n}^{O}_{M}$	$^{avail}\bar{n}^{O}_{M}$	f_M	r_{MM} (min) (Å)	Reference
AlP_3O_9	1	6	6	0	5.19	[33]
	1	6	6	0	4.60	[34]
$AlPO_4$	3	4	4	0	4.45	[35]
$Y_2P_4O_{13}$	1.5	7	5	2/7	3.86	[36]
YP_3O_9	1	6	6	0	5.04–5.41	[37]
YPO_4	3	8	4	1/2	3.76	[38, 39]
ErP_5O_{14}	0.6	8	8	0	5.52–5.70	[40, 41]
ErP_3O_9	1	6	6	0	5.37	[42]
$ErPO_4$	3	8	4	1/2	3.74	[39, 43]
LaP_5O_{14}	0.6	8	8	0	5.25	[44]
LaP_3O_9	1	8	6	1/4	4.31	[45]
$LaPO_4$	3	9	4	5/9	4.09–4.17	[39, 46, 47]

(the presence of paramagnetic rare-earth ions in phosphate glasses leads to broadening and degradation of the MAS NMR spectra [17, 18]). Furthermore, the information thus provided will enable a comparison to be made with the structure of La_2O_3–Al_2O_3–P_2O_5 glasses when La_2O_3 is systematically replaced by Al_2O_3 at fixed P_2O_5 content [19]. La^{3+} is also non-paramagnetic and is representative of rare-earth ions from the *large* radius end of the rare-earth series. Since the coordination number of a small or large rare-earth ion in a phosphate crystal or glass of fixed composition is usually rather different (see table 1 and [20, 21]), the replacement of R^{3+} by Al^{3+} should lead to a significant change in the composition dependence of any rare-earth clustering.

A generic model for the structure of phosphate glasses [22–24], which has been extended to give additional information on the clustering of modifying cations [14], is summarized in section 2. The essential theory required to understand the neutron diffraction results is then given in section 3. The sample preparation is outlined in section 4 along with the sample characterization methods which include differential scanning calorimetry, thermal gravimetric analysis and measurement of the Vickers hardness. In section 4, the neutron diffraction and ^{27}Al and ^{31}P MAS NMR methods are also outlined. The neutron diffraction work made use of the time-of-flight instrument GEM [25] at the ISIS pulsed neutron source which accesses a large maximum scattering vector and thereby gives excellent resolution of the glass structure in real-space. The expected P–O, Al–O and Y–O nearest-neighbour distances are also significantly different i.e. the neutron diffraction experiments should resolve the nearest-neighbour real-space peaks. The experimental results are presented in section 5 and are discussed in section 6 by reference to the structural model described in section 2.

2. Structural model for phosphate glasses

In crystalline and glassy P_2O_5, a network is built from corner-sharing PO_4 tetrahedra comprising one terminal oxygen atom, O_T, and three bridging oxygen atoms, O_B, where the P–O distances are $\simeq$1.4 and 1.6 Å respectively [24, 26–30]. The atomic fraction of chemical species α is defined by $c_\alpha = N_\alpha/N$ where N_α is the number of atoms of type α and $N = \Sigma_\alpha N_\alpha$ is the total number of atoms in the system e.g. $c_P = 2/7$ and $c_O = 5/7$ for pure P_2O_5. In the model that has been developed for phosphate glasses [22–24], the addition of a network modifying cation M in the form of an oxide, such as M_2O, MO or M_2O_3, leaves the PO_4 tetrahedra intact but depolymerizes the phosphate network through the breakage of P–O_B–P bonds. This increases the fraction of O_T atoms to which the modifying cations bind via P–O_T–M linkages. Specifically, if y oxygen atoms from the network modifier are added per P_2O_5 unit, the P:O_B:O_T ratio changes from 2:3:2 in pure P_2O_5 to $2:(3-y):2(1+y)$ in the modified material where $y = 2c_O/c_P - 5$ i.e. the network connectivity is dependent on the oxygen-to-phosphorus ratio. The overall O–(P)–O nearest-neighbour coordination number, where the notation refers to oxygen atoms interlinked by phosphorus, is therefore given by

$$\bar{n}^{O}_{O} = \frac{(3-y)}{(5+y)}\bar{n}^{O}_{O_B} + \frac{2(1+y)}{(5+y)}\bar{n}^{O}_{O_T} \qquad (1)$$

where $\bar{n}^{O}_{O_B} = 6$ and $\bar{n}^{O}_{O_T} = 3$ such that $\bar{n}^{O}_{O} = 24/(5+y)$ [23]. Since P–O_B bonds are longer than P–O_T bonds, the mean O–(P)–O distance associated with bridging sites is anticipated to be longer than for terminal sites. The nearest-neighbour P–(O_B)–P coordination number is given by $\bar{n}^{P}_{P} = 3 - y$.

The PO_4 tetrahedra can be classified by using the Q^n terminology where n (= 0, 1, 2, 3) represents the number of P–(O_B)–P linkages per tetrahedron and the charge on a Q^n species is given by $(n-3)e$ where e is the elementary charge [24]. At a given sample composition, the average value of n is therefore equal to the P–(O_B)–P coordination number i.e. $\langle n \rangle = 3 - y$. In a simple ionic model, which provides a guide for understanding the distribution of Q^n sites in phosphate glasses [22, 24, 31, 32], the network first depolymerizes so that the Q^3 species of pure P_2O_5 ($y = 0$) are converted to Q^2 species, a process that is completed at the metaphosphate composition where $y = 1$. For this first composition range $\langle n \rangle = 2f(Q^2) + 3f(Q^3)$, where $f(Q^n)$ denotes the fraction of Q^n tetrahedra ($f(Q^2) + f(Q^3) = 1$), and it follows that

$$f(Q^2) = y \qquad (2a)$$

$$f(Q^3) = 1 - y. \qquad (2b)$$

As more modifier is added, the Q^2 species subsequently convert to Q^1, a process that is completed at the pyrophosphate composition where $y = 2$. For this second composition range $\langle n \rangle = f(Q^1) + 2f(Q^2)$ where $f(Q^1) + f(Q^2) = 1$ and it follows that

$$f(Q^2) = 2 - y \qquad (3a)$$

$$f(Q^1) = y - 1. \qquad (3b)$$

Finally, as yet more modifier is added the Q^1 species subsequently convert to Q^0 species, a process that is completed at the orthophosphate composition where $y = 3$. For this third

composition range $\langle n \rangle = f(Q^1)$ where $f(Q^0) + f(Q^1) = 1$ and it follows that

$$f(Q^1) = 3 - y \tag{4a}$$

$$f(Q^0) = y - 2. \tag{4b}$$

Glasses for which $0 \leqslant y < 1$ are referred to as ultraphosphates and those for which $y > 1$ are referred to as polyphosphates [24].

In the case of a monovalent modifying cation M^+, for which the system composition can be written as $(M_2O)_x(P_2O_5)_{1-x}$ $(0 \leqslant x \leqslant 1)$, or a divalent modifying cation M^{2+}, for which the system composition can be written as $(MO)_x(P_2O_5)_{1-x}$, it follows that $y = x/(1-x)$ so that equations (2*a*)–(4*b*) can be re-written accordingly. For these cases the metaphosphate, pyrophosphate and orthophosphate compositions correspond to x values of 1/2, 2/3 and 3/4, respectively. By contrast, in the case of a trivalent modifying cation M^{3+} the system composition can be written as $(M_2O_3)_x(P_2O_5)_{1-x}$ and it follows that $y = 3x/(1-x)$. Equations (2*a*)–(4*b*) can be re-written accordingly and the metaphosphate, pyrophosphate and orthophosphate compositions now correspond to $x = 1/4$, 2/5 and 1/2, respectively. We note that the expressions for $f(Q^n)$ given by equations (2*a*)–(4*b*) have to be adjusted if the Q^n species in the melt from which the glass is formed reorganize according to equilibrium relations such as [22, 24, 32]

$$2Q^2 \rightleftharpoons Q^1 + Q^3 \tag{5a}$$

$$2Q^1 \rightleftharpoons Q^0 + Q^2 \tag{5b}$$

which satisfy the necessary charge balance conditions. This site disproportionation is reduced, i.e. the equilibrium reactions in equations (5*a*) and (5*b*) are forced to the left-hand side, as the M–O_T interaction takes a more ionic character in order to produce a more uniform spatial distribution of modifying cations [22, 32].

In the model of Hoppe and co-workers [23], all of the terminal oxygen atoms O_T tend to coordinate to a network modifying cation and form M–O_T–P bridges. Often the modifying cations bind exclusively to O_T atoms as in the case of the crystal structures for the trivalent cations given in table 1. In this scenario it follows that if the mean coordination number of the modifying cation, $\bar{n}^{\rm O}_{\rm M}$, is greater than the number of O_T atoms available per modifying cation, ${}^{\rm avail}\bar{n}^{\rm O}_{\rm M}$, where

$${}^{\rm avail}\bar{n}^{\rm O}_{\rm M} = 2\left[c_{\rm O} - 2c_{\rm P}\right]/c_{\rm M}, \tag{6}$$

then O_T atoms must be shared between the modifying cations. Hence a measure of the number of O_T atoms bound to a modifying cation that are shared between M-centred coordination polyhedra is given by the ratio $f_{\rm M} = (\bar{n}^{\rm O}_{\rm M} - {}^{\rm avail}\bar{n}^{\rm O}_{\rm M})/\bar{n}^{\rm O}_{\rm M}$. It follows that [8]

$$f_{\rm M} = 1 - \frac{2\left[c_{\rm O} - 2c_{\rm P}\right]}{c_{\rm M}\bar{n}^{\rm O}_{\rm M}} \tag{7}$$

leading to the values for crystalline rare-earth phosphates given in table 1. In general, when $f_{\rm M} > 0$ shorter M–M distances are observed since O_T atoms have to be shared between M-centred coordination polyhedra. This is illustrated by the comparison of the different Y–P–O crystal structures given in table 1. In some cases it is also possible to deduce simple expressions for the corresponding nearest-neighbour M–M coordination number in terms of $f_{\rm M}$. For example, if the M-centred coordination polyhedra share only edges and the O_T atoms are solely two-fold coordinated then $\bar{n}^{\rm M}_{\rm M} = f_{\rm M}\bar{n}^{\rm O}_{\rm M}$ which gives the measured $\bar{n}^{\rm M}_{\rm M}$ values of 2, 4, 4 and 2 for the crystal structures of $Y_2P_4O_{13}$ [36], YPO_4 [38, 39], $ErPO_4$ [39, 43] and LaP_3O_9 [45] respectively. By comparison, in the case of crystalline $LaPO_4$ the product $f_{\rm M}\bar{n}^{\rm O}_{\rm M} = 5$ but there are either (i) edge-sharing configurations of M-centred coordination polyhedra in which both two- and three-fold coordinated O_T atoms occur such that $\bar{n}^{\rm M}_{\rm M} = 6$ [39, 46] or (ii) combinations of edge- and face-sharing M-centred coordination polyhedra in which two- and three-fold coordinated O_T atoms can also occur such that $\bar{n}^{\rm M}_{\rm M} = 5$ [47].

Often, a second type of modifier is added to a phosphate network in order to produce a glass with the desired properties. For example, the use of Al_2O_3 as a second modifier can increase both the chemical durability and glass transition temperature and decrease the thermal expansion coefficient [13]. Let R and Al denote the two different types of modifying cation where $c_{\rm M} = c_{\rm R} + c_{\rm Al}$. Then the number of O_T atoms available per modifying cation M is given by equation (6) and of these atoms the fraction required by R is given by $c_{\rm R}\bar{n}^{\rm O}_{\rm R}/c_{\rm M}$ and the fraction required by Al is given by $c_{\rm Al}\bar{n}^{\rm O}_{\rm Al}/c_{\rm M}$. Thus if there are neither Al–O_T–Al nor Al–O_T–R linkages and O_T atoms coordinated by three M atoms do not occur, the number of O_T atoms available to $c_{\rm R}/c_{\rm M}$ atoms of R is given by $\{2[c_{\rm O} - 2c_{\rm P}] - c_{\rm Al}\bar{n}^{\rm O}_{\rm Al}\}/c_{\rm M}$ where $\bar{n}^{\rm O}_{\rm Al}$ is the Al–O coordination number. Hence the number of O_T atoms available to a single atom of R is ${}^{\rm avail}\bar{n}^{\rm O}_{\rm R} = \{2[c_{\rm O} - 2c_{\rm P}] - c_{\rm Al}\bar{n}^{\rm O}_{\rm Al}\}/c_{\rm R}$ and the fraction of O_T atoms bonded to R that are shared between R-centred coordination polyhedra is given by [14] $f_{\rm s} \equiv (\bar{n}^{\rm O}_{\rm R} - {}^{\rm avail}\bar{n}^{\rm O}_{\rm R})/\bar{n}^{\rm O}_{\rm R}$ where

$$f_{\rm s} = 1 - \frac{2\left[c_{\rm O} - 2c_{\rm P}\right] - c_{\rm Al}\bar{n}^{\rm O}_{\rm Al}}{c_{\rm R}\bar{n}^{\rm O}_{\rm R}}. \tag{8}$$

The assumption of no Al–O_T–Al linkages is supported by experiment and will be discussed in sections 5 and 6. Equation (8) reduces to (7) when the second modifier is not present.

For an oxygen atom in a regular AlO_6 octahedron, there are four oxygen atom nearest-neighbours at a distance $\sqrt{2}r_{\rm AlO}$ and one further oxygen atom at a distance $2r_{\rm AlO}$ where $r_{\rm AlO} = 1.88$ Å is a typical Al–O bond distance [33]. Let y oxygen atoms be added to P_2O_5 to give a total of $5 + y$ oxygen atoms (i.e. $(3-y)O_B$ and $2(1+y)O_T$) in a glass having a ratio of 2P to $2c_{\rm Al}/c_{\rm P}$ Al. Then if all of the Al atoms in the material form AlO_6 octahedra, $6 \times 2c_{\rm Al}/c_{\rm P}$ of the oxygen atoms will each have 4 oxygen nearest-neighbours in an octahedron at a distance $\sqrt{2}r_{\rm AlO} = 2.66$ Å. The corresponding O–(Al)–O coordination number is given by $\bar{n}^{\rm O}_{\rm O} = 48c_{\rm Al}/(5+y)c_{\rm P}$ [14]. By comparison, if all of the Al atoms in the material form regular AlO_4 tetrahedra then $4 \times 2c_{\rm Al}/c_{\rm P}$ of the oxygen atoms will have three oxygen

nearest-neighbours at a distance $\sqrt{8/3}r_{\mathrm{AlO}} = 2.87$ Å where $r_{\mathrm{AlO}} = 1.76$ Å is a typical Al–O bond distance [48]. The corresponding O–(Al)–O coordination number is given by $\bar{n}^{\mathrm{O}}_{\mathrm{O}} = 24c_{\mathrm{Al}}/(5+y)c_{\mathrm{P}}$. In alumino-phosphate framework structures, irregular AlO_5 polyhedra occur that are intermediate between trigonal bipyramids and tetragonal pyramids with a mean Al–O distance $r_{\mathrm{AlO}} = 1.83$ Å [49]. Within the AlO_5 polyhedron, an oxygen atom has three nearest-neighbour oxygen atoms between 2.58 and 3.05 Å and one further oxygen atom at 3.38–3.47 Å. For the nearest-neighbours, an O–(Al)–O coordination number given by $\bar{n}^{\mathrm{O}}_{\mathrm{O}} = 30c_{\mathrm{Al}}/(5+y)c_{\mathrm{P}}$ at a distance of ≈2.74 Å is therefore anticipated if all of the Al atoms in the material form AlO_5 structural motifs.

3. Neutron diffraction theory

In a neutron diffraction experiment on a Y–Al–P–O glass, the coherent intensity can be represented by the total structure factor [50]

$$F(k) = \sum_{\alpha}\sum_{\beta} c_\alpha c_\beta b_\alpha b_\beta \left[S_{\alpha\beta}(k) - 1\right] \tag{9}$$

where c_α and b_α denote the atomic fraction and bound coherent scattering length of chemical species α and $S_{\alpha\beta}(k)$ denotes a Faber–Ziman partial structure factor. The accompanying real-space information is contained in the total pair-correlation function

$$D(r) = \frac{4\pi n_0 r}{|G(0)|}G(r) \tag{10}$$

where n_0 is the atomic number density,

$$G(r) = \sum_{\alpha}\sum_{\beta} c_\alpha c_\beta b_\alpha b_\beta \left[g_{\alpha\beta}(r) - 1\right], \tag{11}$$

and $g_{\alpha\beta}(r)$ is a partial pair-distribution function. The limiting value $G(0)$ follows from setting $g_{\alpha\beta}(0) = 0$ in equation (11). In a diffraction experiment, $D(r)$ is seldom obtained directly from the measured total structure factor because of the finite measurement window of the diffractometer $M(k \leqslant k_{\max}) = 1$, $M(k > k_{\max}) = 0$ which is represented in real-space by the symmetrical function

$$M(r) = \frac{1}{\pi}\int_0^{k_{\max}} \mathrm{d}k \cos(kr) = \frac{1}{\pi r}\sin(k_{\max}r). \tag{12}$$

Instead, the function $D'(r)$ is obtained where

$$\begin{aligned} D'(r) &= \frac{2}{\pi|G(0)|}\int_0^{\infty} \mathrm{d}k F(k) k M(k) \sin(kr) \\ &= D(r) \otimes M(r) \end{aligned} \tag{13}$$

and $\otimes$ denotes the one-dimensional convolution operator. The normalization by $|G(0)|$ ensures that the weighting factors of the $g_{\alpha\beta}(r)$ in equations (10) and (13) sum to unity such that $D(r)$ or $D'(r)$ is given by $-4\pi n_0 r$ at small-r values.

To enable those features that are an artefact of $M(r)$ to be distinguished, each peak i in $rg_{\alpha\beta}(r)$ can be represented by a Gaussian centred at $r_{\alpha\beta}(i)$ having a standard deviation $\sigma_{\alpha\beta}(i)$ and an area which corresponds to a coordination number $\bar{n}^{\beta}_{\alpha}(i)$ of species β around α. The measured $D'(r)$ can then be fitted by least squares to a sum of these Gaussians convoluted with $M(r)$ such that

$$\begin{aligned} D'(r) = \sum_i \Bigg[&\frac{W_{\alpha\beta}(i)\bar{n}^{\beta}_{\alpha}(i)}{\sqrt{2\pi}c_\beta(i)r_{\alpha\beta}(i)\sigma_{\alpha\beta}(i)} \\ &\times \exp\left(\frac{-(r - r_{\alpha\beta}(i))^2}{2\sigma^2_{\alpha\beta}(i)}\right) \otimes M(r)\Bigg] - 4\pi n_0 r \end{aligned} \tag{14}$$

where $W_{\alpha\beta}(i) = c^2_\alpha b^2_\alpha/|G(0)|$ if $\alpha = \beta$ and $W_{\alpha\beta}(i) = 2c_\alpha c_\beta b_\alpha b_\beta/|G(0)|$ if $\alpha \neq \beta$. In general, the peaks fitted at the larger-r values are not expected to yield accurate parameters, owing to the overlap from correlations at even larger-r, but are included in order to increase the reliability of the parameters that are reported for the peaks fitted at smaller-r.

4. Experimental method

4.1. Glass preparation and characterization

Yttrium alumino-phosphate glasses were prepared by fusing Y_2O_3 (99.99%) and Al_2O_3 (99.99%) with P_2O_5 (99.99%) in alumina crucibles (Anderman). The dry oxide powders were mixed in a ratio M_2O_3:P_2O_5 of 0.15:0.85 (where M denotes Y and/or Al) to ensure an excess of P_2O_5 relative to the metaphosphate composition, and most of this excess sublimed during the heating procedure. The powder mixtures (of mass ≈25 g) were initially allowed to absorb a small amount (≈100 mg) of atmospheric water at room temperature before the crucible with its lid were placed into a preheated oven at 500 °C for 1 h. The crucible was then moved to another oven at 1000 °C, left for 30 min, and finally transferred to a third oven at 1620 °C. After 30 min the melt was poured into a preheated graphite mould and annealed at 500 °C for 24 h. The resultant glasses were transparent, free from bubbles and visibly homogeneous.

Although all of the glasses were prepared by using an identical method, the crucibles were not sealed and the process by which the Al is incorporated into the glassy matrix is not controlled. The glass compositions were therefore analysed by using electron probe microanalysis (EPMA). In the latter experiments, a cross section was taken through each sample to examine the bulk material at several points and the glass composition was thereby found to be microscopically homogeneous. Factors aiding the preparation of homogeneous samples are, presumably, the use of a small sample volume, which gives rise to a large contact area between the melt and crucible surface, and the fluidity of the melt at the high temperatures utilized, which helps to distribute the alumina dissolved at the crucible surface throughout the bulk material. The glass compositions are given in table 2 together with the mass density which was obtained by measuring the weight of a sample in fluids (air, water and acetone) of different density.

The glass transition temperature T_{g}, melting point temperature T_{mp}, enthalpy of melting H_{mp}, and mass loss on heating were measured by using a TA Instruments SDT Q600 machine which performed simultaneous differential scanning calorimetry (DSC) and thermal gravimetric analysis (TGA). Each finely powdered glass sample of mass ≈20 mg was

Table 2. The composition of the yttrium alumino-phosphate glasses, expressed in terms of the mole fraction of the components, together with the mass density ρ (± 0.01 g cm^{-3}), glass transition temperature T_g (± 2 °C), melting point temperature T_{mp} (± 2 °C), enthalpy of melting H_{mp} (± 1 J g^{-1}), weight loss W_{loss} ($\pm 0.2\%$) and Vickers hardness H_V (± 15 kg mm^{-2}).

Glass	Y_2O_3	Al_2O_3	P_2O_5	ρ (g cm^{-3})	T_g (°C)	T_{mp} (°C)	H_{mp} (J g^{-1})	W_{loss} (%)	H_V (kg mm^{-2})
A	0.000	0.343(3)	0.657(3)	2.53	742	1223	114	1.8	792
B	0.066(3)	0.234(60)	0.700(10)	2.55	704	—	—	3.8	582
C	0.116(4)	0.189(3)	0.694(5)	2.62	707	—	—	12.5	499
D	0.167(5)	0.124(10)	0.709(10)	2.68	698	—	—	9.5	455
E	0.242(6)	0.083(6)	0.674(6)	2.84	730	1231	56	1.8	423
F	0.263(5)	0.026(3)	0.711(2)	2.84	736	1233	21	3.0	410

contained in an alumina crucible and was initially preheated to just above T_g in order to remove thermal stress. It was then heated over the temperature range 50–1500 °C at a rate of 20 °C min^{-1} and the accompanying weight loss for this temperature range was recorded.

The Vickers hardness, H_V, of the glasses was measured by using a diamond pyramid indentation method with a Leco Microhardness testing machine. The sample surface was polished, the instrument was operated with a test load of 1 kg for an indentation time of 30 s, and ten indentations were made per sample. The Vickers hardness is the ratio of the load applied to an indentor to the surface area of the micro-indentation and was calculated by using $H_V = 1.854\ F/d^2$ where F is the load in kg and d is the mean diagonal length of the indentation in mm [51].

4.2. The ^{27}Al and ^{31}P MAS NMR experiments

^{27}Al has a spin 5/2 nucleus and thus has a nuclear quadrupole moment arising from a non-spherically symmetric charge distribution which interacts with the electric field gradient that originates from surrounding charges [52–54]. The resonance peaks are, in general, broad and asymmetric and it is advantageous to make the ^{27}Al MAS NMR experiments at two or more high magnetic fields so that the parameters describing the spectra can be determined more accurately by fitting the measured line shapes. High magnetic fields are necessary in order to resolve the resonance peaks. The two-field spectra were recorded by using (i) a Varian-Chemagnetics CMX 600 MHz Infinity spectrometer with a 14.1 T magnetic field operating at a frequency of 156.33 MHz with a Varian 3.2 mm probe rotating at a frequency of ≈20 kHz, and (ii) a Varian-Chemagnetics CMX 800 MHz Infinity spectrometer with a 18.8 T magnetic field operating at a frequency of 208.57 MHz with a Varian 3.2 mm probe rotating at a frequency of ≈16 kHz. ^{31}P has a spin 1/2 nucleus with a spherical charge distribution. The ^{31}P MAS NMR spectra were recorded by using a Varian-Chemagnetics CMX 360 MHz Infinity spectrometer with a 8.45 T magnetic field operating at a frequency of 145.85 MHz with a Varian 4 mm probe rotating at a frequency of ≈12 kHz.

The ^{27}Al spectra were collected using a one-pulse experiment with either a 0.5 μs (600 MHz spectra) or 0.7 μs (800 MHz spectra) pulse length corresponding to a small tip angle pulse of $<\pi/8$ with a pre-acquisition delay of 7.5 μs. A 1 s repetition time was used and no saturation was observed. Spectra were referenced to the octahedral resonance of $Y_3Al_5O_{12}$ at 0.7 ppm. The ^{31}P spectra were also collected using a one-pulse experiment with a 0.8 μs pulse length corresponding to a $\pi/6$ tip angle with a pre-acquisition delay of 15 μs. A 10 s repetition time was used and no saturation was observed. Spectra were referenced to the resonance of ammonium dihydrogen phosphate $NH_4H_2PO_4$ at 0.9 ppm.

4.3. The neutron diffraction experiments

Neutron diffraction experiments were performed on the glasses labelled A–D and F in table 2 by using the GEM instrument at the ISIS pulsed neutron source [25] with $k_{max} = 49.5$ Å^{-1}. The coarsely powdered samples were held at ambient temperature (≈25 °C) in cylindrical vanadium cans of 8.8 mm internal diameter and 0.1 mm wall thickness and diffraction patterns were taken for the samples in their container, the empty container, the empty instrument, and a vanadium rod of diameter 8.34 mm for normalization purposes. Each complete diffraction pattern was built up from the intensities measured for the different detector groups. These intensities were saved at regular intervals and no deviation between them was observed, apart from the expected statistical variations, which verified the diffractometer stability [55]. It was checked that each measured $F(k)$ obeys the sum-rule relation $\int_0^\infty F(k)k^2\,\mathrm{d}k = 2\pi^2 n_0 G(0)$ and gives rise to a well-behaved real-space function $D'(r)$ [50, 56]. This should oscillate about $-4\pi n_0 r$ at small r-values and, when the measured oscillations are set to this expression, the Fourier back-transform of $D'(r)$ should be in good overall agreement with the original reciprocal space data set. The coherent neutron scattering lengths $b_Y = 7.75(2)$, $b_{Al} = 3.449(5)$, $b_P = 5.13(1)$ and $b_O = 5.803(4)$ fm were taken from Sears [57] and the weighting factors for the $S_{\alpha\beta}(k)$ in equation (9) are given in table 3.

5. Results

5.1. Physical properties

The measured thermal parameters for the different glasses are summarized in table 2 along with the Vickers hardness values measured at room temperature. The quoted T_g values correspond to mid-point temperatures and the T_{mp} and H_{mp} parameters are not listed for samples B–D because the melting transition could not be clearly identified. On the absolute temperature scale, $T_g/T_{mp} \approx 2/3$ for the other samples which

Table 3. The weighting factors (in mbarn) for the $S_{\alpha\beta}(k)$ in equation (9). The composition of the glasses is listed in table 2.

Glass	Y–Y	Y–O	Y–P	Y–Al	Al–Al	Al–O	Al–P	P–P	P–O	O–O
A	—	—	—	—	1.408(4)	29.75(5)	8.01(2)	11.39(4)	84.6(2)	157.2(2)
B	0.252(1)	12.66(3)	3.56(1)	0.800(2)	0.636(2)	20.13(3)	5.66(1)	12.61(5)	89.6(2)	159.2(2)
C	0.798(4)	22.52(6)	6.30(2)	1.156(3)	0.419(1)	16.31(3)	4.56(1)	12.43(5)	88.9(2)	158.9(2)
D	1.620(8)	32.16(9)	9.12(3)	1.076(3)	0.1788(5)	10.68(2)	3.031(7)	12.84(5)	90.5(2)	159.6(2)
F	4.03(2)	50.7(1)	14.41(5)	0.358(1)	0.0080(2)	2.256(4)	0.641(2)	12.90(5)	90.8(2)	159.7(2)

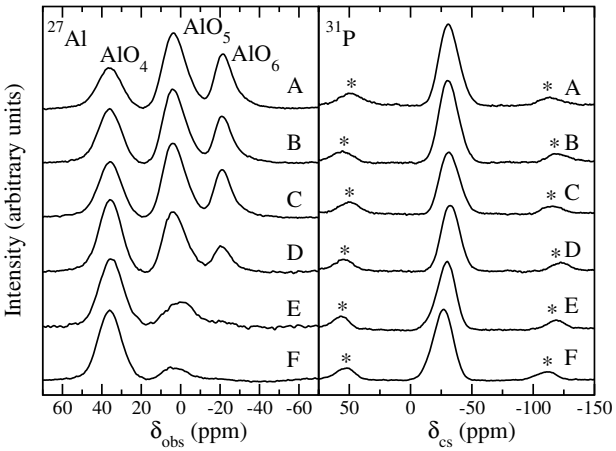

Figure 1. The ^{27}Al and ^{31}P MAS NMR spectra recorded for the Y–Al–P–O glasses labelled A–F in table 2. The ^{27}Al spectra, given in the column on the left-hand side, were measured by using the 800 MHz spectrometer with a magnetic field of 18.8 T. The peaks corresponding to the AlO_4, AlO_5 and AlO_6 coordination environments are identified. The ^{31}P spectra are given in the column on the right-hand side and the spinning sidebands are indicated by asterisks.

is consistent with the empirical rule of Kauzmann [58]. T_g is a maximum when there is either no Y_2O_3 or minimal Al_2O_3 and there is generally a larger mass loss during heating for compositions in between. H_V shows a monotonic increase with increasing Al_2O_3 content and its value surpasses that for silica ($H_V = 714$ kg mm^{-2} [59]) when no Y_2O_3 is present.

5.2. Nuclear magnetic resonance

Several of the measured MAS NMR spectra are shown in figure 1 and, for each glass, the isotropic chemical shift δ_{cs} and full-width at half-maximum of the measured ^{31}P line shape are listed in table 4. The ^{31}P spectra could not be clearly resolved into their contributions from the different Q^n species which precluded an accurate interpretation of the data. This difficulty is consistent with work on e.g. high aluminium content sodium alumino-phosphate glasses [60, 61] and points towards a blurring of distinction between the various PO_4 tetrahedra. For example, in the case of metaphosphate glasses there is a trend for the full-width at half-maximum of a ^{31}P peak to increase with field strength of the modifying cation (as estimated by the cation valence divided by the square of its radius) which is consistent with an increase in the distribution of bond lengths and angles [24, 62]. Although the field strength is not the only relevant parameter [63, 64], a change in character of the PO_4 tetrahedra is supported by neutron diffraction experiments on metaphosphate glasses which show a loss in ability to observe splitting of the first P–O peak in $D'(r)$ [64–66]. For example, it is possible to resolve the first P–O peak into its contributions from the P–O$_T$ and P–O$_B$ correlations in the case of glassy KPO_3 but it is more difficult in the case of glassy LaP_3O_9 or AlP_3O_9. The last observation is consistent with the neutron diffraction results obtained in the present work (see below). An interpretation of the phosphorus coordination environment would benefit from the application of homonuclear two-dimensional NMR experiments to give information on the connectivity of a Q^n unit to its nearest-neighbours [67]. Also, the INADEQUATE (incredible natural abundance double quantum transfer experiment) approach can be used to give additional information on the different P–O$_B$–P chain lengths in complex phosphate mixtures [68].

The ^{27}Al MAS NMR spectra of figure 1 show three clearly resolved peaks at 33–36 ppm, 0–5 ppm and -(15–22) ppm and there are no clear features to suggest the presence of Al–O–Al bonds [69, 70]. For example, there is no peak or shoulder at 60–63 ppm or at 27–29 ppm corresponding to the Al(OAl)$_4$ and Al(OAl)$_5$ units in amorphous alumina films [71] where the Al(OAl)$_p$ notation refers to Al having p (= 4, 5 or 6) oxygen nearest-neighbours and p aluminium next nearest-neighbours. Amorphous alumina also has a peak at −5–3 ppm due to Al(OAl)$_6$ units but this structural motif is unlikely to occur in the present Y–Al–P–O glasses e.g. the structure of amorphous $AlPO_4$, which has a large Al content, is dominated by Al(OP)$_4$ structural motifs and there is no evidence for Al–O–Al linkages [61, 72, 73]. In accordance with previous work on alumino-phosphate glasses [69], the peaks in the ^{27}Al MAS NMR spectra at 33–36 ppm, 0–5 ppm and -(15–22) ppm were therefore attributed to aluminium in Al(OP)$_4$, Al(OP)$_5$ and Al(OP)$_6$ coordination environments, respectively. The measured peak positions do not, however, give the isotropic chemical shifts. Instead, the centre of gravity δ_{obs} of the measured peaks in the ^{27}Al MAS NMR spectra, which describe transitions between states described by magnetic quantum numbers $m = \pm 1/2$, is shifted relative to the isotropic chemical shift δ_{cs} by the isotropic second-order quadrupolar shift [53, 54, 74]

$$\delta_{Q,\mathrm{iso}}(\mathrm{ppm}) = -\frac{3\left[I(I+1)-3/4\right]}{40I^2(2I-1)^2}\left(1+\frac{\eta^2}{3}\right)\frac{\chi_Q^2}{\nu_0^2}\times 10^6 \tag{15}$$

where $\delta_{obs} = \delta_{cs} + \delta_{Q,iso}$, I is the nuclear spin (= 5/2 for ^{27}Al), η is related to the asymmetry of the electric field gradient at the nucleus, χ_Q is the quadrupolar coupling constant and ν_0 is the resonance frequency. Isotropic chemical shifts δ_{cs} are anticipated for Al(OP)$_4$ in the range 35–48 ppm [52, 75–77],

Table 4. Parameters obtained from the measured ^{31}P and ^{27}Al MAS NMR spectra. The isotropic chemical shift δ_{cs} (taken to be the peak position) and full-width at half-maximum FWHM of the measured line shape are reported for the ^{31}P MAS NMR results. For each AlO_n species ($n = 4$, 5 or 6) the isotropic chemical shift δ_{cs}, mean quadrupolar coupling constant $\bar{\chi}_Q$, width of the quadrupolar distribution $\Delta\chi_Q$, width of the additional broadening Δ and relative peak area RA are reported for the ^{27}Al MAS NMR results. The latter were obtained by using the program QuadFit [78] to simultaneously fit the ^{27}Al spectra recorded at two different magnetic fields (see the text). The width Δ depends on the magnetic field so values are quoted for the spectra recorded at both 14.1 and 18.8 T. The errors are, unless otherwise stated, ±1 ppm on δ_{cs} and ±1 ppm on FWHM for the ^{31}P spectra together with ±3 ppm on δ_{cs}, ±0.5 MHz on $\bar{\chi}_Q$, ±0.5 MHz on $\Delta\chi_Q$ and ±20 Hz on Δ for the ^{27}Al spectra. The error on RA is $\pm3\%$ for samples A, C–F and $\pm4\%$ for sample B. The mean coordination number $\bar{n}^{O}_{Al}$ of oxygen around Al, as calculated from the ^{27}Al NMR results, is also quoted.

Glass	δ_{cs} (^{31}P) (ppm)	FWHM (ppm)	Unit	δ_{cs} (ppm)	$\bar{\chi}_Q$ (MHz)	$\Delta\chi_Q$ (MHz)	Δ^a (Hz)	Δ^b (Hz)	RA (%)	$\bar{n}^{O}_{Al}$
A	−31	19	AlO_4	41	6.0	1.9	470	720	25	5.0(1)
			AlO_5	9	6.4	3.9	470	570	48	
			AlO_6	−17	5.6	5.0	290	420	27	
B	−30	19	AlO_4	40	5.4	1.6	480	730	32	4.9(1)
			AlO_5	10	6.4	3.9	430	540	46	
			AlO_6	−17	5.6	4.7	280	400	22	
C	−32	19	AlO_4	40	5.8	2.2	450	710	33	4.9(1)
			AlO_5	9	6.5	3.9	410	530	45	
			AlO_6	−18	5.3	4.8	270	420	22	
D	−32	18	AlO_4	41	5.5	1.9	490	670	46	4.7(1)
			AlO_5	10	6.4	4.1	440	530	41	
			AlO_6	−16	4.9	4.0	300	420	13	
E	−30	17	AlO_4	41	6.0	2.1	500	690	69	4.3(1)
			AlO_5	7	6.0	5.0	540	750	28	
			AlO_6	−18	4(1)	3(1)	350	470	3	
F	−27	19	AlO_4	42	5.8	2.2	510	680	81	4.2(1)
			AlO_5	9	6.2	4.8	470	720	17	
			AlO_6	−16	6(1)	2(1)	510	680	2	

[a] Fit at 14.1 T.
[b] Fit at 18.8 T.

for $Al(OP)_5$ in the range 10–16 ppm [52, 76, 77], and for $Al(OP)_6$ in the range -(15–25) ppm [52, 77]. For brevity of notation, these species will henceforth be referred to as AlO_n where n is 4, 5 or 6.

When Al-centred structural motifs are distorted, as in the case of AlO_n units in glass, the ^{27}Al nucleus will experience a range of local coordination environments. Since the quadrupolar coupling constant depends on the electric field gradient at the nucleus, there will be an accompanying spread of measured χ_Q values. The measured ^{27}Al MAS NMR spectra were therefore simulated by using the program QuadFit [78] which assumes a second-order quadrupolar line shape with a distribution of interaction parameters. A Gaussian distribution of the quadrupolar coupling constant about a mean value was taken along with an additional Gaussian broadening which takes into account other effects such as a small distribution of δ_{iso} values. The asymmetry parameter η was assumed to be zero. An iterative method was used to obtain a set of parameters that give the best simulation of the measured spectra recorded at both magnetic fields. An example of the fitted spectra for glass A is given in figure 2. The fitted values for the isotropic chemical shift, mean quadrupolar coupling constant $\bar{\chi}_Q$, full-width at half-maximum of the quadrupolar coupling constant distribution $\Delta\chi_Q$, full-width at half-maximum of the additional Gaussian broadening Δ, and relative peak area for each AlO_n species are summarized in table 4. The full-width at half-maximum of the additional

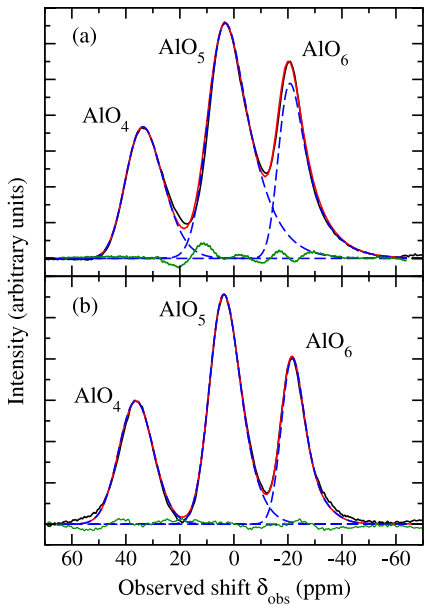

Figure 2. The ^{27}Al MAS NMR spectra for glass A (solid black curves) as measured by using (a) the 600 MHz spectrometer with a magnetic field of 14.1 T and (b) the 800 MHz spectrometer with a magnetic field of 18.8 T. The fitted peaks corresponding to the AlO_4, AlO_5 and AlO_6 coordination environments are given by the broken (blue) curves and the overall fit is given by the light solid (red) curve. The difference between the data and overall fit is given by the solid (green) curve oscillating about the horizontal line at the base of each spectrum.

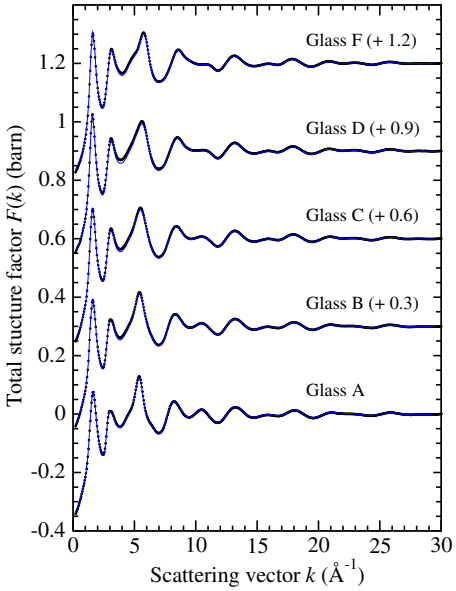

Figure 3. The total structure factors, $F(k)$, for the Y–Al–P–O glasses labelled A–D and F as measured by using neutron diffraction at ≈25 °C. The solid circles give the data points and the symbol size is larger than the error bars. The solid (blue) curves are the Fourier back-transforms of the corresponding $D'(r)$ (see figure 4) after the unphysical low-r oscillations have been set to the calculated value of $-4\pi n_0 r$. The data sets have been truncated at 30 Å^{-1} for clarity of presentation and the Fourier back-transforms are almost indistinguishable from the data points at most k-values.

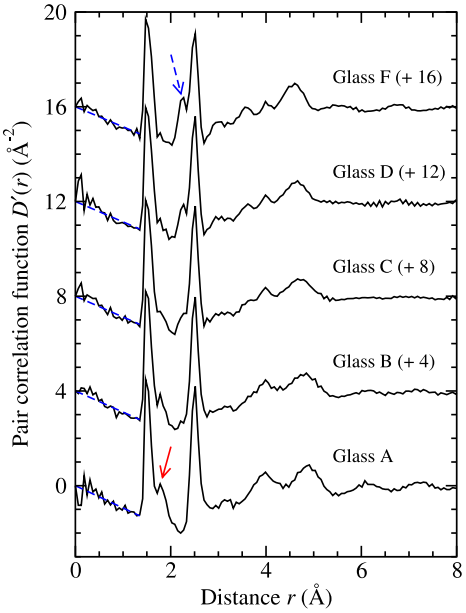

Figure 4. The total pair-correlation function, $D'(r)$, for the Y–Al–P–O glasses labelled A–D and F as obtained by Fourier transforming the $F(k)$ functions shown in figure 3 by using equation (13) with $k_{max} = 49.5$ Å^{-1}. For each function the broken (blue) curve at low-r gives the limiting values as calculated from $-4\pi n_0 r$. The lower solid (red) arrow points to the nearest-neighbour Al–O correlations at ≈1.8 Å and the upper broken (blue) arrow points to the nearest-neighbour Y–O correlations at 2.25(1) Å.

Gaussian broadening Δ is small by comparison with $\Delta\chi_Q$. The values for δ_{cs} reported in table 4 are in good accord with the ^{27}Al MAS NMR results of Buckermann *et al* [77] who found isotropic chemical shifts of 40, 10 and -16 ppm for the AlO_4, AlO_5 and AlO_6 coordination environments, respectively, in glassy $(Al_2O_3)_x(P_2O_5)_{1-x}$ with x values of 0.25 and 0.30.

5.3. Neutron diffraction

The total structure factors measured by using neutron diffraction are shown in figure 3 and the corresponding pair-correlation functions $D'(r)$ are shown in figure 4. As the Y_2O_3 content is increased on progressing from sample A to F, the Al–O peak in $D'(r)$ at ≈1.8 Å decreases in intensity while a peak due to Y–O correlations appears at 2.25(1) Å [36, 37] and increases in intensity. The first few peaks in the $D'(r)$ functions were fitted by using equation (14) and several of the results are shown in figure 5. In this fitting procedure the Al–O coordination numbers were fixed in accordance with the ^{27}Al NMR results e.g. $\bar{n}^{O}_{Al} = 4 \times 0.25 = 1$ for the AlO_4 units of sample A where the relative peak area RA = 0.25 is given in table 4. The fitted parameters are summarized in table 5 and the goodness-of-fit parameter R_χ is defined in [79]. In addition, the nearest-neighbour O–(Al)–O correlations for glass A were estimated by fitting $D'(r)$ and $\bar{n}^{O}_{O}$ values of 0.9(2), 1.0(2) and 0.4(2) were obtained for Gaussian peaks centred at 2.66(1), 2.75(2) and 2.84(2) Å respectively. On the basis of the structural model, the O–(Al)–O coordination number for a given type of polyhedron is obtained by multiplying the

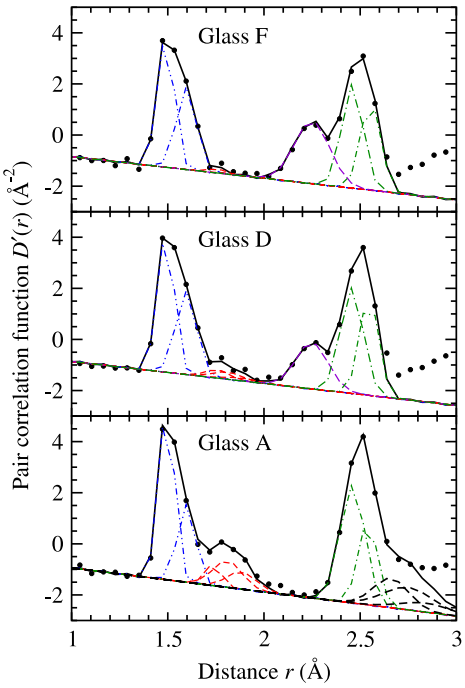

Figure 5. The filled circles give the total pair-correlation function, $D'(r)$, shown in figure 4 for the glasses labelled A, D and F. The solid (black) curves give the fitted function and the other curves give the individual convoluted Gaussians: P–O (— · · — (blue)), Al–O (- - - - (red)), Y–O (– – – (violet)) and O–(P)–O (— · — (green)). For glass A there are no Y–O correlations and the convoluted Gaussians for the O–(Al)–O correlations (– – – (black)) are shown at the largest r-values.

Table 5. Parameters obtained from the Gaussian fits to the total pair-correlation function $D'(r)$ measured for the yttrium alumino-phosphate glasses labelled A–D and F in table 2. Typical errors are ±0.1 on the coordination number $\bar{n}_\alpha^\beta$, ±0.01 Å on the peak position $r_{\alpha\beta}$ and ±0.009 Å on the standard deviation $\sigma_{\alpha\beta}$. The goodness-of-fit parameter R_χ [79] is quoted for a fit range of 1.0–2.6 Å.

Glass	Parameter	P–O_T	P–O_B	AlO_4[a]	AlO_5[a]	AlO_6[a]	Y–O	O–(P)–O	O–(P)–O	R_χ (%)
A	$\bar{n}_\alpha^\beta$	2.44	1.36	1.00	2.40	1.62	—	2.35	1.31	6.2
	$r_{\alpha\beta}$ (Å)	1.49	1.60	1.74	1.81	1.88	—	2.46	2.54	
	$\sigma_{\alpha\beta}$ (Å)	0.040	0.047	0.042	0.075	0.075	—	0.065	0.050	
B	$\bar{n}_\alpha^\beta$	2.13	1.59	1.28	2.30	1.32	6.00	2.18	1.64	6.2
	$r_{\alpha\beta}$ (Å)	1.49	1.59	1.74	1.81	1.89	2.25	2.46	2.54	
	$\sigma_{\alpha\beta}$ (Å)	0.041	0.056	0.044	0.057	0.075	0.105	0.065	0.050	
C	$\bar{n}_\alpha^\beta$	2.20	1.58	1.32	2.25	1.32	5.90	2.20	1.59	4.6
	$r_{\alpha\beta}$ (Å)	1.49	1.60	1.76	1.81	1.88	2.25	2.46	2.55	
	$\sigma_{\alpha\beta}$ (Å)	0.043	0.051	0.050	0.084	0.076	0.091	0.058	0.044	
D	$\bar{n}_\alpha^\beta$	2.15	1.70	1.84	2.05	0.78	5.85	2.08	1.67	4.3
	$r_{\alpha\beta}$ (Å)	1.49	1.60	1.76	1.81	1.88	2.25	2.46	2.55	
	$\sigma_{\alpha\beta}$ (Å)	0.043	0.053	0.060	0.076	0.084	0.083	0.059	0.049	
F	$\bar{n}_\alpha^\beta$	2.11	1.69	3.24	0.85	0.12	5.75	2.00	1.67	6.2
	$r_{\alpha\beta}$ (Å)	1.49	1.60	1.76	1.81	1.88	2.25	2.46	2.56	
	$\sigma_{\alpha\beta}$ (Å)	0.043	0.051	0.045	0.044	0.064	0.091	0.055	0.052	

[a] The $\bar{n}_{Al}^O$ values were fixed in accordance with the ^{27}Al MAS NMR results (see text).

Table 6. The glass transition temperature T_g, isotropic chemical shift δ_{cs} from ^{31}P MAS NMR, relative area RA of 4-, 5- and 6-fold coordinated Al and corresponding mean Al–O coordination number $\bar{n}_{Al}^O$ from ^{27}Al MAS NMR for several amorphous $(Al_2O_3)_x(P_2O_5)_{1-x}$ materials as prepared by using a melt-quench (MQ) or sol–gel (SG) method. An uncertainty of ±5% was assumed on the RA values quoted in [19] for evaluating the error on $\bar{n}_{Al}^O$ and the uncertainty on the RA values associated with [72] is ±2%. The measured $\bar{n}_{Al}^O$ values are compared with the number of O_T atoms available per Al, $^{avail}\bar{n}_{Al}^O$, which is given by equation (6).

x	Method	T_g (°C)	δ_{cs} (^{31}P) (ppm)	RA (%) AlO_4	RA (%) AlO_5	RA (%) AlO_6	$\bar{n}_{Al}^O$	$^{avail}\bar{n}_{Al}^O$	Reference
0.25	MQ	—	−40(1)	—	—	—	—	6.00	[77]
0.27	MQ	814(3)	—	9	30	61	5.5(2)	5.70	[19]
0.30	MQ	—	−39(1)	—	—	—	—	5.33	[77]
0.32	MQ	754(3)	—	22	36	42	5.3(2)	5.13	[19]
0.33	MQ	—	−36.4(3)	32	33	35	5.03(6)	5.00	[72]
0.33	SG	—	−37.0(3)	27	29	44	5.17(6)	5.00	[72]
0.343	MQ	742(2)	−31(1)	25	48	27	5.0(1)	4.92	present work
0.40	SG	—	−30.8(3)	63	19	18	4.55(6)	4.50	[72]
0.50	SG	1060(10)	−25.9(3)	91	3	4	4.03(7)	4.00	[61, 72, 73]

relevant formula for $\bar{n}_O^O$ given in section 2 by the RA value for that polyhedron type as provided by the ^{27}Al NMR results (see table 4). $\bar{n}_O^O$ values of 1.03 at 2.66 Å, 1.17 at 2.74 Å and 0.48 at 2.87 Å are thereby calculated for the AlO_4, AlO_5 and AlO_6 units of glass A, respectively, in fair agreement with the experimental data.

6. Discussion

There have been several studies of $(Al_2O_3)_x(P_2O_5)_{1-x}$ glasses using ^{27}Al and ^{31}P MAS NMR [19, 61, 72, 77, 80] and several of the results are summarized in table 6. A systematic shift in the value of δ_{cs} (^{31}P) is observed with increasing alumina content which is consistent with phosphorus taking an increasing number of Al next nearest-neighbours. The mean Al–O coordination number is in agreement, within the experimental error, with the prediction of the structural model given by equation (6) which is consistent with the observations made by Brow *et al* [80]. The glasses display the 'range II' behaviour described by Hoppe *et al* [64] i.e. the mean coordination number of Al^{3+} decreases with increasing modifier content in order to match the number of available O_T atoms. For the $(Al_2O_3)_x(P_2O_5)_{1-x}$ glasses prepared by conventional bulk-quenching methods, T_g decreases with increasing Al_2O_3 content as the mean Al–O coordination number decreases (see table 6). As a point of reference, $T_g \approx 380\,°C$ for vitreous P_2O_5 [81].

In table 7, several of the coordination numbers measured for the Y–Al–P–O glasses are compared to those obtained from the model of section 2. The close overall agreement demonstrates that the model can act as an excellent starting point for understanding the structure of phosphate glasses, even when they contain four different chemical species. This observation is corroborated by previous neutron diffraction experiments in which the method of isomorphic substitution was used to study the structure of R–Al–P–O glasses with R = Dy and/or Ho [7, 8, 20] and the structure of R–Al–P–O glasses with R = La and/or Ce [14, 20].

Table 7. Comparison of the parameters expected from the model described in section 2 and those obtained from the Gaussian fits to $D'(r)$.

Parameter	Origin	Glass A	Glass B	Glass C	Glass D	Glass F
y	—	1.569	1.283	1.322	1.232	1.220
$\bar{n}_{\mathrm{P}}^{\mathrm{O_T}}$	Model	2.57	2.28	2.32	2.23	2.22
	Fit	2.4(1)	2.1(1)	2.2(1)	2.2(1)	2.1(1)
$\bar{n}_{\mathrm{P}}^{\mathrm{O_B}}$	Model	1.43	1.72	1.68	1.77	1.78
	Fit	1.4(1)	1.6(1)	1.6(1)	1.7(1)	1.7(1)
$\bar{n}_{\mathrm{O}}^{\mathrm{O}}$ [O–(P)–O]	Model	3.65	3.82	3.80	3.85	3.86
	Fit	3.7(1)	3.8(1)	3.8(1)	3.8(1)	3.7(1)

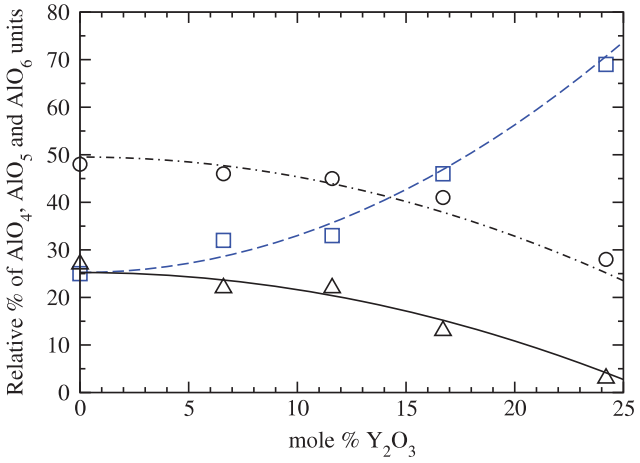

Figure 6. The relative percentage of AlO_4 (squares), AlO_5 (circles) and AlO_6 (triangles) units in the Y–Al–P–O glasses, as obtained from the relative peak areas of the ^{27}Al MAS NMR spectra (see table 4), plotted as a function of the Y_2O_3 content. At each composition, the relative percentages of the units sum to give 100%. The error bars are comparable to the symbol size and the curves are shown as guides to the eye.

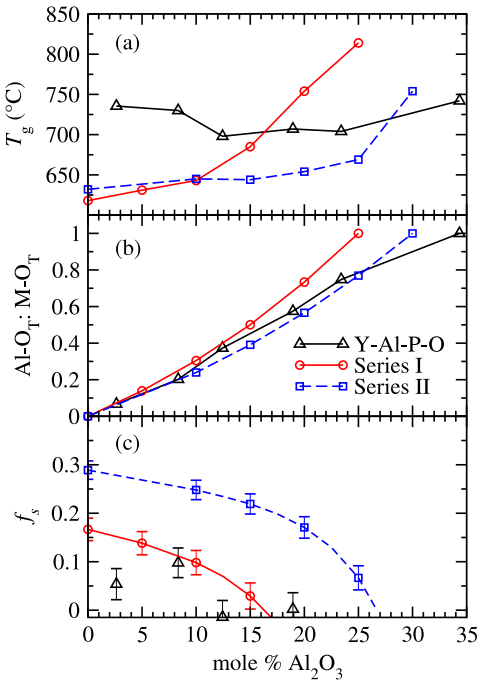

Figure 7. A comparison between (a) the glass transition temperature T_g, (b) the bond ratio Al–O_T:M–O_T and (c) the parameter f_s (as calculated by using equation (8)) for the Y–Al–P–O glasses of the present work and for two series of La–Al–P–O glasses investigated by Karabulut *et al* [19]. The present work (open triangles) corresponds to glasses of nominal composition $(M_2O_3)_{0.31}(P_2O_5)_{0.69}$ where M denotes Y and/or Al. The work of Karabulut *et al* [19] corresponds to glasses of nominal composition $(M_2O_3)_x(P_2O_5)_{1-x}$ where M denotes La and/or Al with $x = 0.25$ for series I (open circles) and $x = 0.30$ for series II (open squares). The data sets are plotted as a function of the Al_2O_3 content of the glass which increases as R_2O_3 is replaced by Al_2O_3 at fixed total modifier M_2O_3 content. The f_s values and Al–O_T:M–O_T bond ratios were deduced by using the $\bar{n}_{\mathrm{Al}}^{\mathrm{O}}$ values taken from ^{27}Al MAS NMR experiments together with $\bar{n}_{\mathrm{Y}}^{\mathrm{O}} = 5.9$ (present work), $\bar{n}_{\mathrm{La}}^{\mathrm{O}} = 7.2$ (series I) or $\bar{n}_{\mathrm{La}}^{\mathrm{O}} = 7.5$ (series II)—further details for the La–Al–P–O glasses are given in [14]. The effect of varying the $\bar{n}_{\mathrm{R}}^{\mathrm{O}}$ values by ± 0.2 is shown by the error bars on the f_s values in (c), and is smaller than the symbol size in (b). The curves are shown as guides to the eye.

The ^{27}Al MAS NMR results in table 4 show that the mean coordination number $\bar{n}_{\mathrm{Al}}^{\mathrm{O}}$ decreases from a value of 5.0(1) as aluminium is replaced by yttrium in the Y–Al–P–O series of glasses while the neutron diffraction results in table 5 give a mean coordination number $\bar{n}_{\mathrm{Y}}^{\mathrm{O}} = 5.9(2)$, averaged for all of the yttrium containing glasses. As shown in figure 6, the reduction in $\bar{n}_{\mathrm{Al}}^{\mathrm{O}}$ arises from a decrease in the number of AlO_6 and AlO_5 units relative to AlO_4 units i.e. Y^{3+} preferentially replaces those Al^{3+} ions having higher coordination numbers. As discussed in section 5.2, there is no clear evidence from the ^{27}Al NMR spectra for Al–O–Al conformations in any glass from the Y–Al–P–O series. The results are therefore consistent with a picture in which yttrium preferentially bonds to the available O_T atoms in order to fulfil its bonding requirements and the coordination number of Al adjusts to avoid Al–O_T–Al linkages. As Y_2O_3 replaces Al_2O_3 in the Y–Al–P–O series of glasses, the mean Al–O_T coordination number first decreases since there are fewer O_T atoms available to aluminium. A composition is then reached where there are insufficient O_T atoms to accommodate separated Y-centred coordination polyhedra. At this point, sharing occurs between the O_T atoms of these polyhedra and the f_s values calculated from equation (8) for glasses C–F, using $\bar{n}_{\mathrm{Y}}^{\mathrm{O}} = 5.9(2)$ and the NMR results for $\bar{n}_{\mathrm{Al}}^{\mathrm{O}}$, are shown in figure 7(c). For samples E and F, $f_s > 0$ and $y \approx 1.2$ (see table 7) which compares to $f_s = 2/7 = 0.29$ and $y = 1.5$ for crystalline $Y_2P_4O_{13}$ [36] (see table 1). It is therefore anticipated that the shortest Y–Y nearest-neighbour distance for samples E and F will be comparable to the crystalline phase value of ≈3.86 Å which

corresponds to edge-sharing polyhedra. The accompanying Y–Y coordination number, deduced from $\bar{n}^{Y}_{Y} = f_s \bar{n}^{O}_{Y}$ (see section 2), is estimated to be in the range 0.3(2)–0.6(2).

By comparison, Karabulut *et al* [19] studied two series of $(M_2O_3)_x(P_2O_5)_{1-x}$ glasses where M was chosen to be La, Al or a mixture of the two. The nominal O:P ratio was fixed at 3.0 for series I, corresponding to $x = 0.25$ and $y = 1$, and at 3.143 for series II, corresponding to $x = 0.30$ and $y = 1.286$. The results were also interpreted in terms of a model in which there is preferential bonding of La^{3+} to O_T atoms and an avoidance of Al–O_T–Al linkages. Since $\bar{n}^{O}_{La} > \bar{n}^{O}_{Al}$ [14] it follows that the replacement of Al^{3+} by La^{3+} at fixed total modifier (M^{3+}) content will decrease the number of O_T atoms available per Al^{3+}. The Al–O_T coordination number should therefore decrease if Al–O_T–Al bonds are to be avoided and this trend was observed in the ^{27}Al NMR experiments of Karabulut *et al* [19]. Furthermore, glasses from series II have, by comparison with those from series I, less O_T atoms available per modifier ion at 5.33 compared to 6. Preferential bonding of O_T by La^{3+} will therefore leave less O_T available for Al^{3+} and, as observed in the NMR experiments [19], the series II glasses should have smaller $\bar{n}^{O}_{Al}$ values. The f_s values for series I and II were estimated by Martin *et al* [14] and the results are summarized in figure 7(c). Series II has a similar nominal composition to the $(M_2O_3)_{0.31-x}(P_2O_5)_{0.69}$ set of Y–Al–P–O glasses but the La–O_T coordination number is larger than the Y–O_T coordination number since $\bar{n}^{O}_{La} \approx 7.5$ and $\bar{n}^{O}_{Y} \approx 5.9$. In consequence, there is more necessity for O_T atoms to be shared between La-centred coordination polyhedra for small Al_2O_3 content glasses and, as a result, the f_s values are larger.

As illustrated in figure 7(a), T_g for the Y–Al–P–O set of glasses shows little dependence on the Al_2O_3 content by comparison to T_g for series I and II of the La–Al–P–O glasses. It is therefore of interest to examine the dependence of T_g on the type of modifying cation. The Al–O_T:M–O_T ratio, where M denotes R or Al, can be obtained from the expression $c_{Al}\bar{n}^{O}_{Al}/(c_R\bar{n}^{O}_{R} + c_{Al}\bar{n}^{O}_{Al})$. In the case of the La–Al–P–O glasses, this bond ratio increases most rapidly with Al_2O_3 content for the glasses of series I (see figure 7(b)) which correlates with a more rapid rise of T_g by comparison with series II. The results are therefore consistent with a network modifying role for Al^{3+} in La–Al–P–O glasses where it helps to strengthen the glass through the formation of O_T–Al–O_T linkages [14]. Indeed, Al^{3+} often has a strengthening effect on phosphate networks [13]. However, in the case of the Y–Al–P–O glasses, T_g is comparable for both the low and high Al_2O_3 content glasses i.e. Al^{3+} does not have a marked strengthening role in these materials, as measured by its effect on T_g, although the Vickers hardness V_H of the glasses does increase with aluminium content (see table 2). It is notable that, for the La–Al–P–O glasses, T_g for each series increases most rapidly with increasing Al_2O_3 content only after f_s has reached a minimal value. It therefore appears that the strength of these glasses is also dependent on the connectivity of the La-centred coordination polyhedra which is reduced by the replacement of La^{3+} by Al^{3+} [14].

Lastly, rare-earth phosphate glasses are of widespread interest, due in part to their applications, and as outlined in section 1 the information provided for Y–Al–P–O glasses can be applied to help increase our understanding of these rare-earth materials. Mountjoy and co-workers [82] have pointed out that the nearest-neighbour R–R distance of 5.62(6) Å reported by Martin *et al* [7, 8] for the glassy rare-earth phosphate $(R_2O_3)_{0.230}(Al_2O_3)_{0.069}(P_2O_3)_{0.701}$, with R = Dy and/or Ho, is incompatible with the value of $f_s = 0.19$ as calculated from equation (8) by using coordination numbers of $\bar{n}^{O}_{R} = 6.7$ (corresponding to two peaks at 2.30(1) and 2.67(1) Å with $\bar{n}^{O}_{R}$ coordination numbers of 6.2(1) and 0.5(1) respectively) and $\bar{n}^{O}_{Al} = 5.5$ which were obtained by fitting the neutron diffraction results. This finite f_s value implies a sharing of O_T atoms between R-centred coordination polyhedra. The associated R–R distance is expected to be ≈3.9 Å for edge-sharing conformations (see table 1) and its maximum value is ≈4.97 Å which corresponds to a linear R–O_T–R conformation where the two different nearest-neighbour R–O distances of 2.30 and 2.67 Å are added. It is therefore conceivable that the peak observed at 4.72(2) Å in $d_{RR}(r)$ for the Dy/Ho glass, which yields a coordination number $\bar{n}^{R}_{R} \approx 1.0$, is in fact a genuine structural feature as opposed to a Fourier transform artefact [7, 8]. Indeed, a comparable nearest-neighbour Sm–Sm distance of ≈4.6–4.8 Å is reported for a glass of nominal composition $(Sm_2O_3)_{0.2}(P_2O_5)_{0.8}$ containing Al impurities [10, 11]. However, the measured coordination number $\bar{n}^{O}_{Sm} = 6.9(2)$ leads to $f_s = 0$ for this particular glass i.e. there is no need for O_T atoms to be shared between Sm-centred coordination polyhedra. Also, an R–R distance as long as 4.72(2) Å is not expected if an O_T atom shares two R atom nearest-neighbours [21]. It is therefore notable that a reduced value of $f_s = 0.04$ is calculated for the Dy/Ho glass by using $\bar{n}^{O}_{R} = 6$ and $\bar{n}^{O}_{Al} = 4.3$ as estimated from the results of the present work. Thus a plausible scenario for the Dy/Ho glass is an f_s value which is smaller than originally estimated, corresponding to a short R–R distance of ≈3.9 Å that could not be identified, together with a longer R–R distance of 4.72(2) Å between those R-centred coordination polyhedra that do not share a common O_T atom. A broad range of R–R distances then follows, corresponding to the main peak in $d_{RR}(r)$ at 5.62(6) Å.

7. Conclusions

Neutron diffraction and NMR experiments were made on a series of $(M_2O_3)_x(P_2O_5)_{1-x}$ glasses with M = Y and/or Al and $x \approx 0.31$. The results are in excellent overall accord with the generic structural model for phosphate glasses summarized in section 2 and support a picture in which the modifying Y^{3+} cations preferentially bind to the available O_T atoms in order to fulfil their bonding requirements. The f_s parameter, which measures the connectivity of the Y-centred coordination polyhedra, can be reduced by substituting Y_2O_3 by Al_2O_3 at fixed total modifier content x. These observations support the results previously obtained for two sets of $(M_2O_3)_x(P_2O_5)_{1-x}$ glasses from the large radius end of the rare-earth series with $x = 0.25$ or 0.30 and M = La and/or Al [8, 19]. At a given composition, f_s takes a larger value when the glass contains La^{3+} instead of Y^{3+} ions, in accordance with the larger

coordination number of La^{3+}. A route is thereby provided for understanding the basic structure of rare-earth phosphate glasses and for controlling rare-earth clustering.

Acknowledgments

We thank Gavin Mountjoy (Kent) for useful discussions, Anita Zeidler (Bath) for assistance with the crystallography, Hugh Perrot (Bath) for the electron probe microanalysis of the samples, and Hellmut Eckert and Long Zhang (Münster) for providing the relative areas for their ^{27}Al MAS NMR data given in table 6. We also thank the EPSRC for financial support and acknowledge use of the EPSRC Chemical Database Service.

References

[1] Weber M J 1990 *J. Non-Cryst. Solids* **123** 208
[2] Weber M J 1991 *Materials Science and Technology* vol 9, ed J Zarzycki (Weinheim: VCH) p 619
[3] Marion J E and Weber M J 1991 *Eur. J. Solid State Inorg. Chem.* **28** 271
[4] Rapp C F 1995 *CRC Handbook of Laser Science and Technology (Suppl. 2)* ed M J Weber (Boca Raton, FL: CRC Press) p 619
[5] Davey S T, Ainslie B J and Wyatt R 1995 *CRC Handbook of Laser Science and Technology (Suppl. 2)* ed M J Weber (Boca Raton, FL: CRC Press) p 635
[6] Martin R A and Knight J C 2006 *IEEE Photon. Technol. Lett.* **18** 574
[7] Martin R A, Salmon P S, Fischer H E and Cuello G J 2003 *Phys. Rev. Lett.* **90** 185501
[8] Martin R A, Salmon P S, Fischer H E and Cuello G J 2003 *J. Phys.: Condens. Matter* **15** 8235
[9] Cole J M, Hannon A C, Martin R A and Newport R J 2006 *Phys. Rev.* B **73** 104210
[10] Cole J M, Wright A C, Newport R J, Sinclair R N, Fischer H E, Cuello G J and Martin R A 2007 *J. Phys.: Condens. Matter* **19** 056002
[11] Wright A C, Cole J M, Newport R J, Fisher C E, Clarke S J, Sinclair R N, Fischer H E and Cuello G J 2007 *Nucl. Instrum. Methods Phys. Res.* A **571** 622
[12] Cole J M and Newport R J 2007 *J. Non-Cryst. Solids* **353** 1773
[13] Metwalli E and Brow R K 2001 *J. Non-Cryst. Solids* **289** 113
[14] Martin R A, Salmon P S, Benmore C J, Fischer H E and Cuello G J 2003 *Phys. Rev.* B **68** 054203
[15] Shannon R D 1976 *Acta Crystallogr.* A **32** 751
[16] Pettifor D G 1986 *J. Phys. C: Solid State Phys.* **19** 285
[17] Cole J M, van Eck E R H, Mountjoy G, Newport R J, Brennan T and Saunders G A 1999 *J. Phys.: Condens. Matter* **11** 9165
[18] Cole J M, van Eck E R H, Mountjoy G, Anderson R, Brennan T, Bushnell-Wye G, Newport R J and Saunders G A 2001 *J. Phys.: Condens. Matter* **13** 4105
[19] Karabulut M, Metwalli E and Brow R K 2001 *J. Non-Cryst. Solids* **283** 211
[20] Martin R A, Salmon P S, Fischer H E and Cuello G J 2004 *J. Non-Cryst. Solids* **345/346** 208
[21] Hoppe U, Brow R K, Ilieva D, Jóvári P and Hannon A C 2005 *J. Non-Cryst. Solids* **351** 3179
[22] Van Wazer J R 1958 *Phosphorus and its Compounds* vol 1 (New York: Interscience) chapter 12
[23] Hoppe U 1996 *J. Non-Cryst. Sol.* **195** 138
[24] Brow R K 2000 *J. Non-Cryst. Solids* **263/264** 1
[25] Hannon A C 2005 *Nucl. Instrum. Methods Phys. Res.* A **551** 88
[26] Hoppe U, Walter G, Barz A, Stachel D and Hannon A C 1998 *J. Phys.: Condens. Matter* **10** 261
[27] Hoppe U, Walter G, Kranold R and Stachel D 1998 *Z. Naturf.* a **53** 93
[28] Hoppe U, Kranold R, Barz A, Stachel D and Neuefeind J 2000 *Solid State Commun.* **115** 559
[29] Stachel D, Svoboda I and Fuess H 1995 *Acta Crystallogr.* C **51** 1049
[30] Arbib E H, Elouadi B, Chaminade J P and Darriet J 1996 *J. Solid State Chem.* **127** 350
[31] Kirkpatrick R J and Brow R K 1995 *Solid State Nucl. Magn. Reson.* **5** 9
[32] Walter G, Hoppe U, Vogel J, Carl G and Hartmann P 2004 *J. Non-Cryst. Solids* **333** 252
[33] van der Meer H 1976 *Acta Crystallogr.* B **32** 2423
[34] Fratzky D, Schneider M and Meisel M 2000 *Z. Kristallogr. New Cryst. Struct.* **215** 341
[35] Achary S N, Jayakumar O D, Tyagi A K and Kulshresththa S K 2003 *J. Solid State Chem.* **176** 37
[36] Ivashkevich L S, Lyakhov A S, Selevich A F, Ilieva D and Lesnikovich A I 2002 *Z. Kristallogr.* **217** 605
[37] Graia M, Driss A and Jouini T 2003 *Solid State Sci.* **5** 393
[38] Milligan W O, Mullica D F, Beall G W and Boatner L A 1982 *Inorg. Chim. Acta* **60** 39
[39] Ni Y, Hughes J M and Mariano A N 1995 *Am. Mineral.* **80** 21
[40] Jezowska-Trzebiatowska B, Mazurak Z and Lis T 1980 *Acta Crystogr.* B **36** 1639
[41] Katrusiak A and Kaczmarek F 1995 *Cryst. Res. Technol.* **30** 501
[42] Dorokhova G I and Karpov O G 1984 *Sov. Phys. Crystallogr.* **29** 400
[43] Milligan W O, Mullica D F, Beall G W and Boatner L A 1983 *Acta Crystallogr.* C **39** 23
[44] Cole J M, Lees M R, Howard J A K, Newport R J, Saunders G A and Schönherr E 2000 *J. Solid State Chem.* **150** 377
[45] Matuszewski J, Kropiwnicka J and Znamierowska T 1988 *J. Solid State Chem.* **75** 285
[46] Mullica D F, Milligan W O, Grossie D A, Beall G W and Boatner L A 1984 *Inorg. Chim. Acta* **95** 231
[47] Callejas G, Blanco M, Cabrera S, Prieto O, Luna I, Choque V and Crespo P 2000 *Rev. Boliv. Quim.* **17** 22
[48] Hannon A C and Parker J M 2000 *J. Non-Cryst. Solids* **274** 102
[49] Parise J B and Day C S 1985 *Acta Crystallogr.* C **41** 515
[50] Fischer H E, Barnes A C and Salmon P S 2006 *Rep. Prog. Phys.* **69** 233
[51] Callister W D Jr 2000 *Materials Science and Engineering: An Introduction* 5th edn (New York: Wiley)
[52] Smith M E 1993 *Appl. Magn. Reson.* **4** 1
[53] Kentgens A P M 1997 *Geoderma* **80** 271
[54] Smith M E and van Eck E R H 1999 *Prog. Nucl. Magn. Reson. Spectroc.* **34** 159
[55] Jal J F, Mathieu C, Chieux P and Dupuy J 1990 *Phil. Mag.* B **62** 351
[56] Salmon P S, Xin S and Fischer H E 1998 *Phys. Rev.* B **58** 6115
[57] Sears V F 1992 *Neutron News* **3** 26
[58] Feltz A 1993 *Amorphous Inorganic Materials and Glasses* (Weinheim: VCH) p 51
[59] Kurkjian C R 2000 *J. Non-Cryst. Solids* **263/264** 207
[60] Egan J M, Wenslow R M and Mueller K T 2000 *J. Non-Cryst. Solids* **261** 115
[61] Zhang L and Eckert H 2006 *J. Phys. Chem.* B **110** 8946
[62] Brow R K, Phifer C C, Turner G L and Kirkpatrick R J 1991 *J. Am. Ceram. Soc.* **74** 1287
[63] Rashid N E, Phillips B L and Risbud S H 2000 *J. Mater. Res.* **15** 2463
[64] Hoppe U, Walter G, Kranold R and Stachel D 2000 *J. Non-Cryst. Solids* **263/264** 29

[65] Hoppe U, Walter G, Stachel D and Hannon A C 1995 *Z. Naturf.* a **50** 684
[66] Hoppe U, Kranold R, Stachel D, Barz A and Hannon A C 1998 *J. Non-Cryst. Sol.* **232–234** 44
[67] Jäger C, Hartmann P, Witter R and Braun M 2000 *J. Non-Cryst. Solids* **263/264** 61
[68] Fayon F, King I J, Harris R K, Evans J S O and Massiot D 2004 *C. R. Chim.* **7** 351
[69] Brow R K, Kirkpatrick R J and Turner G L 1990 *J. Am. Ceram. Soc.* **73** 2293
[70] MacKenzie K J D and Smith M E 2002 *Multinuclear Solid-State NMR of Inorganic Materials* (Oxford: Pergamon)
[71] Dupree R, Farnan I, Forty A J, El-Mashri S and Bottyan L 1985 *J. Physique Coll.* **C8** 113
[72] Zhang L and Eckert H 2004 *J. Mater. Chem.* **14** 1605
[73] Zhang L, Bögershausen A and Eckert H 2005 *J. Am. Ceram. Soc.* **88** 897
[74] Jelinek R, Chmelka B F, Wu Y, Grandinetti P J, Pines A, Barrie P J and Klinowski J 1991 *J. Am. Chem. Soc.* **113** 4097
[75] Müller D, Jahn E, Ladwig G and Haubenreisser U 1984 *Chem. Phys. Lett.* **109** 332
[76] Alemany L B, Timken H K C and Johnson I D 1988 *J. Magn. Reson.* **80** 427
[77] Buckermann W A, Müller-Warmuth W and Mundus C 1996 *J. Non-Cryst. Solids* **208** 217
[78] Kemp T F 2004 *MSc Thesis* University of Warwick, UK
[79] Grimley D I, Wright A C and Sinclair R N 1990 *J. Non-Cryst. Solids* **119** 49
[80] Brow R K, Click C A and Alam T M 2000 *J. Non-Cryst. Solids* **274** 9
[81] Hudgens J J and Martin S W 1993 *J. Am. Ceram. Soc.* **76** 1691
[82] Clark E B, Mead R N and Mountjoy G 2006 *J. Phys.: Condens. Matter* **18** 6815